BIOCHEMISTRY

© Copyright 2004 by the American Chemical Society Volume 43, Number 35 September 7, 2004

Accelerated Publications

Stress Sensor Triggers Conformational Response of the Integral Membrane Protein Microsomal Glutathione Transferase 1†

Laura S. Busenlehner,‡ Simona G. Codreanu,‡ Peter J. Holm,§ Priyaranjan Bhakat,§ Hans Hebert,§ Ralf Morgenstern,# and Richard N. Armstrong*,‡

Departments of Biochemistry and Chemistry, Center in Molecular Toxicology, Vanderbilt University School of Medicine, Nashville, Tennessee 37232-0146, Center for Structural Biochemistry, Department of Biosciences at Novum, Karolinska Institutet, SE-141 57 Huddinge, Sweden, Institute of Environmental Medicine, Karolinska Institutet, S-171 77 Stockholm, Sweden

Received June 21, 2004; Revised Manuscript Received July 26, 2004

ABSTRACT: Microsomal glutathione (GSH) transferase 1 (MGST1) is a trimeric, integral membrane protein involved in cellular response to chemical or oxidative stress. The cytosolic domain of MGST1 harbors the GSH binding site and a cysteine residue (C49) that acts as a sensor of oxidative and chemical stress. Spatially resolved changes in the kinetics of backbone amide H/D exchange reveal that the binding of a single molecule of GSH/trimer induces a cooperative conformational transition involving movements of the transmembrane helices and a reordering of the cytosolic domain. Alkylation of the stress sensor preorganizes the helices and facilitates the cooperative transition resulting in catalytic activation.

The membrane-bound microsomal glutathione (GSH)[1] transferase 1 (MGST1) is found in abundance in both the endoplasmic reticulum and outer mitochondrial membranes. The protein is a member of the membrane-associated proteins in eicosanoid and glutathione metabolism (MAPEG) superfamily that includes prostaglandin E_2 synthase, leukotriene C_4 synthase, and 5-lipoxygenase activating protein (*1*). The MGST1 protein is involved in the protection of cells against oxidative damage of membrane lipids by functioning as a peroxidase with lipid hydroperoxides or by catalyzing the addition of GSH to electrophilic species such as epoxides (*2*, *3*). The protein is unique in that its catalytic response is enhanced by oxidation or alkylation of a cysteine residue (C49), which acts as an antenna for the detection of chemical or oxidative stress (*4*).

The protein exists in the membrane as a 52 kDa homotrimer that binds a single molecule of GSH (*5*−*7*). The binding and ionization of GSH occurs in a two-step process involving a rapid-equilibrium association followed by a slow conformational transition ($k = 0.4\ s^{-1}$) and concomitant formation of a tight enzyme−thiolate (E_3*·GS^-) complex as shown in Scheme 1 (*6*). The formation of E_3*·GS^- is often the rate-limiting step in catalysis. Alkylation of the stress sensor (C49) activates the enzyme by increasing the

† Supported by Grants R01 GM30910, P30 ES00267, T32 ES07028, and F32 ES13105 (to L.S.B.) from the National Institutes of Health, the Swedish Cancer Society, the Swedish National Board for Laboratory Animals, funds from the Karolinska Institutet, and Swedish Research Council Grants 00144 and 621/3056.

* Address correspondence to this author. E-mail: r.armstrong@vanderbilt.edu. Fax: 615 343-2921. Tel: 615 343-2920.

‡ Vanderbilt University.

§ Karolinska Institutet, Huddinge.

Karolinska Institutet, Stockholm.

[1] Abbreviations: GSH, reduced glutathione; NEM, *N*-ethylmaleimide; DTNB, 5,5′-dithiobis(2-nitrobenzoic acid); EDTA, ethylenediaminetetraacetic acid; MS, mass spectrometry; ESI, electrospray ionization; TX100, Triton X-100.

10.1021/bi048716k CCC: $27.50 © 2004 American Chemical Society
Published on Web 08/12/2004

Scheme 1

$$E_3 + GSH \underset{}{\overset{50\ mM}{\rightleftharpoons}} E_3{\bullet}GSH \underset{6 \times 10^{-4}\ s^{-1}}{\overset{0.4\ s^{-1}}{\rightleftharpoons}} E_3^*{\bullet}GS^-$$

rate of the conformational transition 30-fold ($k = 13\ s^{-1}$) (*8*).

The three-dimensional structure of MGST1 has been determined to 6 Å resolution by electron crystallography of two-dimensional crystals with plane groups *P*6 (*9*) and $P22_12_1$ (*10*). The three-dimensional molecular density map shows that the trimeric protein spans the membrane with three repeats of a left-handed four-helix bundle motif. The principal difference between the $P22_12_1$ and *P*6 structures is a change in the inclination of the helices. It has been suggested that the different helical tilt angles reflect an intrinsic flexibility of the molecule and represent the conformational transition that occurs during formation of the $E_3^*{\bullet}GS^-$ complex (*10*). The cytosolic domain, which is thought to harbor the GSH binding site and the stress sensor, C49, is not well defined in the density map. As a consequence, there is little information on the exact location of the GSH binding site, the conformational transition that accompanies GSH binding, or the structural link between chemical modification of C49 and enhanced catalysis.

In this report, we extend the resolution of the electron crystal structure to 4.5 Å and describe the use of amide H/D exchange mass spectrometry (MS) to map conformational changes of this integral membrane protein upon binding substrate and on chemical modification of the stress sensor. Amide H/D exchange MS provides for the facile and sensitive detection of changes in solvent accessibility and dynamics of the protein backbone (*11*−*14*) with a good degree of spatial resolution. Although the technique has been applied to model membrane peptides (*15*), it has not been exploited to interrogate a functioning integral membrane protein. We demonstrate here that the technique is particularly well suited for integral membrane proteins and can be extended to include catalytically active two-dimensional protein crystals. Alterations in the exchange kinetics indicate that the binding of GSH results in an extensive ordering of the cytosolic domain of the protein and occurs with a cooperative conformational transition involving movements of the transmembrane helices. The activation of the enzyme by alkylation of the stress sensor poises the protein near the transition and thus facilitates the binding and ionization of GSH under conditions of chemical stress.

EXPERIMENTAL PROCEDURES

Materials. Deuterium oxide (99.9 at. % D), glutathione, β-mercaptoethanol, and pepsin were purchased from Sigma Chemical Co. (St. Louis, MO). *N*-Ethylmaleimide (NEM) was obtained from ICN Biomedicals, Inc. (Aurora, OH) and 5,5′-dithiobis(2-nitrobenzoic acid) from Aldrich Chemical Co. (Milwaukee, WI). Bovine liver L-α-phosphatidylcholine was purchased from Avanti Polar Lipids, Inc. (Alabaster, AL). Formic acid (90%) was supplied by J. T. Baker (Phillipsburg, NJ) and anhydrous monobasic potassium phosphate by Fisher Scientific (Pittsburgh, PA). HPLC grade acetonitrile was purchased from EM Science (Gibbstown, NJ).

Enzyme Preparation. MGST1 was purified from livers of male Sprague-Dawly rats as previously described (*16*) and was stored in 10 mM potassium phosphate (pH 7.0), 0.1 M KCl, 0.1 mM EDTA, 1 mM glutathione, 0.2% Triton X-100, and 20% glycerol. Removal of GSH from MGST1 prior to mass spectrometry was performed with 10 DG gel filtration columns (Bio-Rad Laboratories; Hercules, CA) preequilibrated with 10 mM potassium phosphate (pH 7.0). After addition of MGST1, the protein was eluted with 10 mM potassium phosphate (pH 7.0). Two passes over the gel filtration column were required to remove all contaminating GSH, as confirmed by DTNB-free thiol quantification (*17*). Protein concentration was determined with the noninterfering protein assay (Geno Technology, Inc.; St. Louis, MO) and bovine serum albumin as the standard. Stock protein samples (58 μM; 1.0 mg/mL) for H/D exchange experiments were aliquoted, purged with nitrogen gas, and flash-frozen at −80 °C.

Crystallization, Electron Microscopy, and Data Processing. Two-dimensional crystals of MGST1 with bovine liver L-α-phosphatidylcholine were prepared as previously described (*18*). Electron crystallography was used to determine the three-dimensional structure of MGST1 from two-dimensional crystals having two different symmetries observed earlier, $P22_12_1$ and *P*6 (*19, 20*). The map of the orthorhombic form ($P22_12_1$) was calculated from analysis according to ref *21* and from merging 45 images collected at a specimen temperature of 4 K (*22*) and at tilt angles up to 53°. The overall weighted phase residual and *R*-factor were 23.1° and 0.35, respectively, for data with a cutoff at 4.5 Å resolution. Previous angular correlation tests (*10*) have shown very strong noncrystallographic 3-fold symmetry of the MGST1 trimer in the orthorhombic crystal form, and consequently, this local symmetry operation was imposed to obtain the final map.

The phosphatidylcholine complex of MGST1 for H/D exchange was prepared in the same way as for the two-dimensional crystals. Detergent-solubilized MGST1 was mixed with bovine-liver L-α-phosphatidylcholine at a lipid to protein molar ratio of ∼3 (*18, 19*). The protein concentration in the dialysate was 2 mg/mL. The detergent was removed over 8 days of dialysis at 20 to 30 °C against detergent-free buffer containing 10 mM potassium phosphate (pH 7.0), 50 mM KCl, 0.1 mM EDTA, 20% v/v glycerol, and 1 mM GSH. The final concentration of MGST1 was 1.75 mg/mL.

Identification of Peptic Fragments of MGST1. Prior to H/D exchange experiments, apo-MGST1 was thawed and filtered through a 0.2 μm cellulose acetate spin column (Corning Incorporated; Acton, MA) to remove any particulate matter or insoluble protein. Pepsin digests of apo-MGST1 (1.5:1 pepsin/MGST1 w/w) were performed under the quenching conditions of the H/D exchange experiment (5 min, pH 2.4, 0 °C). Essentially, 17 μg of MGST1 in 100 μL of quench buffer (0.1 M potassium phosphate (pH 2.4)) was digested by adding 25 μg of pepsin (5 μL of 5 mg/mL solution in H_2O) for 5 min on ice. The pepsin-digested peptides were separated by reversed-phase HPLC and identified by tandem ESI-MS/MS sequencing "on the fly" as peptides are eluted. Peptides were first separated on a microbore 1 mm × 150 mm C18 column (Phenomenex, Torrence, CA), using a 5−75% acetonitrile/H_2O gradient over 25 min (0.1 mL/min),

where both mobile phases contained 0.4% formic acid. Peptides were sequenced using a ThermoFinnigan LCQ ion-trap mass spectrometer (San Jose, CA) in positive-ion mode by data-dependent tandem MS/MS collision-induced dissociation. The putative identities of the peptides were determined from a computer-generated peptic peptide map of MGST1 with the ExPASy-PeptideMass software (*23*) and were confirmed by analysis of the MS/MS sequencing of individual peptides by comparison to the theoretical fragmentation patterns for that peptide generated by the ProteinProspector program MS-Product (*24*). Pepsin digests of MGST1 were found to be highly reproducible under the optimized conditions presented. The pepsin-MGST1 peptide map is shown in Figure S1 (Supporting Information).

Hydrogen−Deuterium Exchange. GSH−MGST1 for H/D exchange experiments was prepared by adding 3 mM glutathione [0.1 M potassium phosphate, (pH 7.0)] to apo-MGST1 in complex with Triton X-100 (1.0 mg/mL, 58 μM) or to 2-D crystals of MGST1 (1.7 mg/mL, 98 μM) and allowing the mixture to equilibrate 20 min on ice before use. NEM-alkylated MGST1 was prepared by incubating apo-MGST1 (58 μM) with 120 μM *N*-ethylmaleimide [0.1 M potassium phosphate, (pH 7.0)] on ice for 30 min before each time point to avoid protein aggregation. The alkylation reaction was quenched with 100 μM β-mercaptoethanol prior to deuteration. NEM-alkylated GSH−MGST1 was prepared by incubating apo-MGST1 (58 μM) with 120 μM *N*-ethylmaleimide (0.1 M potassium phosphate (pH 7.0) on ice for 30 min. The reaction was quenched on ice by the addition of 3.2 mM glutathione, which reacts with the remaining free NEM but is in excess so that GSH binds the active site of the protein (*25*).

Deuterium exchange was initiated by the addition of 10 μL of MGST1 (1.0 mg/mL for the TX100 complex; 1.75 mg/mL for the phospholipids complex) to 40 μL of D_2O. The deuterium−protein solution was incubated at 23 °C for various times (15 s to 6 h), after which the exchange reaction was quenched by addition of 50 μL of quench buffer [0.1 M potassium phosphate (pH 2.4) in H_2O; 0 °C] and subsequent transfer to an ice bath. After 25 s of quenching on ice, 1.5 equiv (w/w) of pepsin (5 μL of 5 mg/mL in water) was added, and the digestion was incubated for an additional 5 min on ice. All protein samples for the H/D exchange (15 time points) were prepared individually and run on the same day.

Deuterium Exchange Control Experiments. To determine the extent of artifactual exchange of deuterium that occurred after the acidification (quench) and during the pepsin digestion, a zero-time control ($m_{0\%}$) was performed (*26*). Ten microliters of MGST1 was added to 50 μL of quench buffer at 0 °C, followed by the addition of 40 μL of D_2O. Pepsin was subsequently added (25 μg), and the protein was digested for 5 min on ice, as described. The extent of deuterium incorporation for individual peptides during the digestion step varied between 0% and 5%.

The amount of deuterium that is lost during the HPLC chromatography step can also be determined. A completely deuterated protein sample ($m_{100\%}$) is necessary for this analysis. The usual method for obtaining the fully deuterated sample requires the addition of D_2O at neutral pH and extended incubation at high temperatures (40−60 °C) to partially denature the protein (*26*). However, MGST1 precipitates at these temperatures; therefore, another method was employed. Ten microliters of MGST1 was added to 40 μL of D_2O and incubated at 32 °C for 5 h, after which 50 μL of deuterated quench buffer (0.1 M potassium phosphate, pD 2.4) was added and incubated for an additional 3 h. After incubation, the sample was transferred to ice, digested with pepsin, and analyzed by the normal procedure. The average amount of deuterium lost during HPLC fractionation was 10−25% after normalizing to 100% deuterium incorporation.

HPLC-ESI Mass Spectrometry. HPLC/ESI-MS was used to determine the extent of deuterium incorporation into individual peptides. The HPLC injection loop and all chromatographic buffers were completely submerged in ice−water slurries maintained at 0 °C to minimize deuterium back-exchange with hydrogen. The pepsin-digested peptides were separated over 12 min by a 5−60% acetonitrile/H_2O gradient where both mobile phases contained 0.4% formic acid. The peptides were separated using a ThermoFinnigan Surveyor HPLC (San Jose, CA) equipped with a Phenomenex microbore 1 mm × 50 mm C18 reverse-phase column (Torrence, CA) at 100 μL/min. A six-port divert valve was used to divert early-eluting phosphate salts and late-eluting detergent molecules to waste. Also, an additional wash step (10 min) with a 2-propanol-containing buffer (50% acetonitrile/40% 2-propanol/10% H_2O/0.4% formic acid) was performed after each injection to remove highly hydrophobic/large detergent particles from the column.

Mass spectra were recorded on a ThermoFinnigan TSQ Quantum triple-quadrupole mass spectrometer (Finnigan Corp., San Jose, CA) using positive ion electrospray ionization (ESI). Before each time course, polytyrosine was used to optimize the sheath and auxiliary nitrogen gas pressures, as well as the tube lens voltage at 182.0, 508.0, and 997.0 *m*/*z*. The heated capillary was maintained at 190 °C, and the spray voltage was kept at 3.5 kV. The detector was calibrated to unit resolution, and the data were collected at a scan time of 1 s and a peak width of 0.7 by scanning over 300−1500 *m*/*z*. Data processing was performed using Finnigan Xcaliber software (version 1.2). Peptide ions were located by mass searching, yielding the chromatographic retention profile for each ion. The scans contained within the extracted chromatographic ion profile were averaged to produce a composite spectrum for each ion. MagTran 1.0 beta 9 software developed by Zhang and Marshall (*27*) was used to determine the centroid of the given composite isotope envelope.

Kinetic Analysis. The deuterium content of partially deuterated peptides must be corrected for the gain ($m_{0\%}$) and loss ($m_{100\%}$) of deuterium during analysis (*12*, *27*). The following expression was used to calculate the corrected deuterium content (*D*) of a peptide (*12*):

$$D = \left[N\left(\frac{m_t - m_{0\%}}{m_{100\%} - m_{0\%}} \right) \right] \quad (1)$$

where $m_{0\%}$, m_t, and $m_{100\%}$ are the average molecular masses of the same peptide in the nondeuterated, the partially deuterated at time *t*, and the fully deuterated control samples, respectively. *N* is the total number of exchangeable peptide amide protons less one for the N-terminal amide proton and any proline residues.

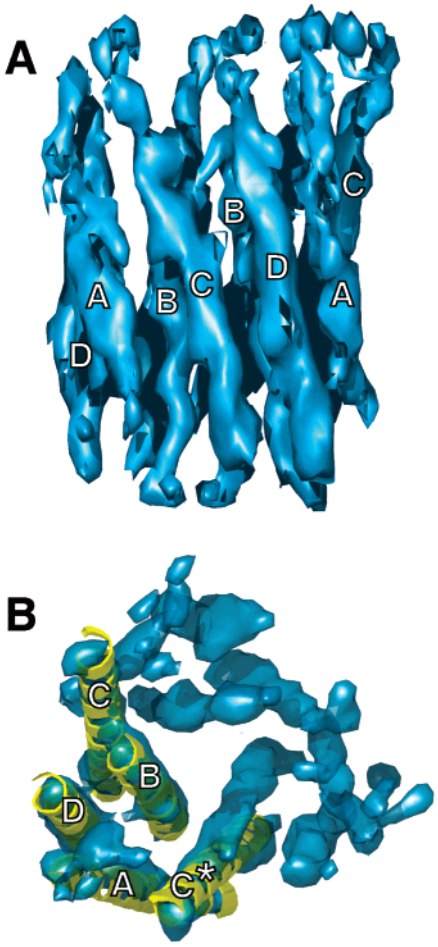

FIGURE 1: Panel A presents a side view of the molecular density map of one trimer of MGST1 at 4.5 Å resolution. The cytosolic domain is on top. A noncrystallographic 3-fold symmetry has been applied as described previously (*10*). Panel B presents a view of one trimer from the unsymmetrized map looking down the noncrystallographic 3-fold axis from the cytosolic side of the membrane. Two possible four-helix bundles for one monomer are illustrated by grouping helical cylinders ABCD or ABC*D. The map was calculated to 4.5 Å resolution from electron micrographs of plane group $P22_12_1$ two-dimensional crystals (*18*) tilted between 0° and 53°. The crystal images were processed using electron and X-ray crystallographic software from the MRC (*28*) and CCP4 (*29*) program systems and visualized using the *O* (*30*), MolRay (*31*) and Povray (*32*) programs.

The amount of deuterium incorporated in each peptide was averaged from three independent kinetic runs and plotted as a function of time. The resulting progress curve for each peptide was fit using KaleidaGraph (Synergy Software) to the sum of first-order rate terms according to eq 2,

$$D = N - A_1 e^{-k_1 t} - A_2 e^{-k_2 t} - A_3 e^{-k_3 t} \ldots - A_n e^{-k_n t} \quad (2)$$

where D is the number of incorporated deuteriums, N is the total number of exchangeable sites, A_n is the number of amide protons that exchange at a given rate constant, k_n, during the time allowed for isotopic exchange, t (*26*). The kinetic profiles were fitted to single-, double-, or triple-exponential equations as appropriate.

RESULTS AND DISCUSSION

Three-Dimensional Structure of MGST1 at 4.5 Å Resolution. The present 3-D map was obtained from a crystallization medium containing glutathione. Exclusion of glutathione does not lead to changes in unit cell dimensions, and it may thus be expected that the structures with and without glutathione are isomorphous. In contrast, soaking preformed 2-D crystals with NEM leads to a gradual disintegration of the periodicity indicating major conformational changes. The molecular density of the orthorhombic crystal form, extended to a resolution of 4.5 Å, is illustrated in Figure 1. Although the connectivity of the helices is still not apparent, the present map shows a clear pitch of the transmembrane helices and some cytosolic substructure (Figure 1A). Consideration of the left-handed twist of typical four-helix bundles in membrane proteins in the absence of information on the helix connectivity suggests that there are two possible groupings of four-helix bundles that comprise a monomer as illustrated in Figure 1B.

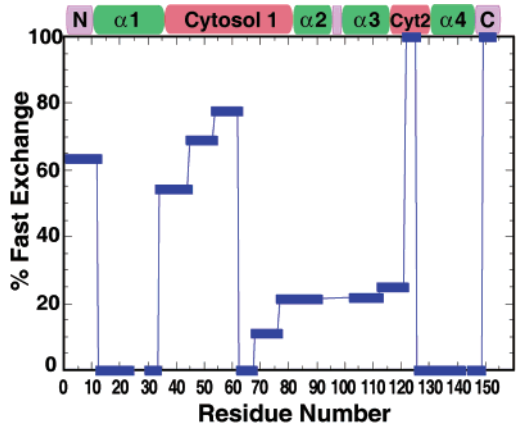

FIGURE 2: Extent of exchange in the fast phase ($k_x > 4$ min^{-1}) as a function of position along the backbone of apoMGST1. The topology of the protein is illustrated at the top where the purple, red, and green segments represent the predicted luminal, cytosolic, and membrane-spanning helical regions, respectively.

Fitting polyalanine helix models into the corkscrew density suggests that the helices vary from 28 to 38 residues with lengths of 33 Å for helix A, 44 Å for helix B, 57 Å for helix C and 39 Å for helix D with an uncertainty in the lengths of between 2 and 5 Å. The longest corkscrew density (helix C) is twice the length necessary to span the phospholipid bilayer. Therefore, it is likely that the helical structure extends into the cytosolic domain. Part of the observed density at the ends of the helices may be due to ordered turns or loops.

Structure and the Kinetics of H/D. To further probe the structure of MGST1, backbone amide H/D exchange kinetics of protein−Triton X-100 (TX100) or protein−phospholipid complexes were measured by pulsing samples with D_2O for times ranging between 15 s and 6 h at 25 °C (pH 7.0). The exchange reactions were quenched (pH 2.4, 0 °C) and rapidly digested with the acid protease pepsin. The extent of isotope incorporation for each of 22 peptides at 15 time points was determined in triplicate by HPLC/ESI-MS. Kinetic profiles for all peptides are given in Figures S2−S17 in Supporting Information.

The extent of fast exchange ($k_x > 4$ min^{-1}) along the protein backbone of apoMGST1 in complex with Triton X-100 (MGST1·TX100) is illustrated in Figure 2. The fast-exchange regime is the best predictor of solvent accessibility and protein secondary structure (*14*). For apo-MGST1, there

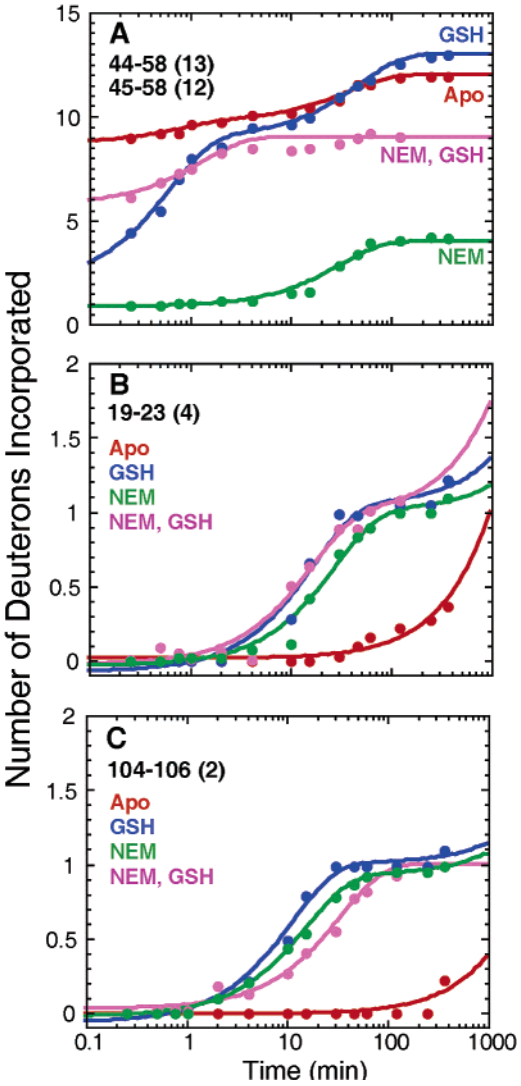

FIGURE 3: Kinetic profiles for H/D exchange of selected peptides in MGST1. The solid lines are fits of the data to either a single- or double-exponential equation. The amplitudes and rate constants used to generate the solid lines are given in Table 1. The number of exchangeable sites for each peptide is shown in parentheses. Panel A shows kinetic profiles for peptide 44−58 from MGST1·TX100 (red) and MGST1·GS$^-$·TX100 (blue). The purple and green traces represent peptide 45−58 from the NEM-alkylated enzyme in the absence and presence of GSH, respectively. Panel B shows kinetic profiles for peptide 19−23 from the MGST1·TX100 (red), MGST1·GS$^-$·TX100 (blue), NEM-alkylated-MGST1·TX100 (purple), and NEM-alkylated-MGST1·GS$^-$·TX100 (green) complexes. Panel C shows kinetic profiles for peptide 104−106 from the MGST1·TX100 (red), NEM-alkylated-MGST1·TX100 (purple), MGST1·GS$^-$·TX100 (blue), and NEM-alkylated-MGST1·GS$^-$·TX100 (green) complexes.

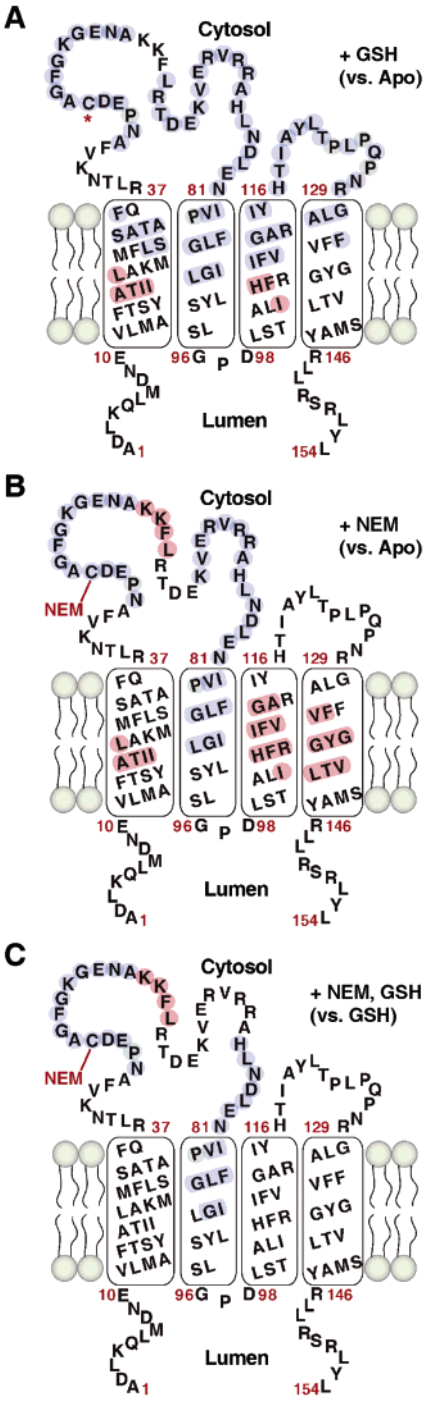

FIGURE 4: Summaries of changes in the H/D exchange kinetics of MGST1 complexes relative to a defined reference state: (A) MGST1·GS$^-$·TX100 referenced to MGST1·TX100. (B) NEM-alkylated MGST1·TX100 referenced to MGST1·TX100. (C) NEM-alkylated MGST1·GS$^-$·TX100 referenced to MGST1·GS$^-$·TX100. The predicted transmembrane helices 1−4 are shown from left to right. Peptides colored in red and blue indicate enhanced and reduced exchange, respectively.

is an excellent correlation between the extent of exchange and the predicted membrane-spanning α-helices. Helices 1 and 4, for example, exhibit no exchange in the fast phase, while about 20% of the sites in the shorter helices 2 and 3 show fast exchange. In contrast, regions in the luminal N- and C-terminal peptides and a significant portion of the cytosolic domain exhibit extensive exchange in the fast phase consistent with considerable solvent exposure of the backbone in these regions.

Influence of GSH on Kinetics of H/D Exchange. The influence of GSH on H/D exchange in the cytosolic domain is marked and illustrated in Figure 3A. Figure 4A provides a summary of all peptides that exhibit a substantial change in exchange behavior upon addition of GSH. A large portion of the cytosolic domain and the C-terminal ends of helices 1 and 3 show decreases in the rate of H/D exchange where at least 30 sites exhibit a significant (>3-fold) reduction (Figure 4A). The profound effect of the addition of GSH on the H/D exchange kinetics signals a substantial conforma-

Table 1: Rate Constants and Amplitudes for H/D Exchange into Selected Peptides of MGST1[a]

peptide/condition[b]	A_1 (D)	k_{x_1} (min^{-1})	A_2 (D)	k_{x_2} (min^{-1})
44−58 (13)/apo	1.1 ± 0.3	1.6 ± 0.6	2.3 ± 0.1	0.026 ± 0.003
44−58 (13)/GSH	7.0 ± 0.5	1.6 ± 0.2	4.0 ± 0.2	0.021 ± 0.002
45−58 (12)/NEM	4.3 ± 0.4	1.6 ± 0.2	4.89 ± 0.09	$\leq 8 \times 10^{-4}$
45−58 (12)/NEM+GSH	3.2 ± 0.1	0.032 ± 0.004		
19−23 (4)/apo	3.99 ± 0.01	$\leq 3 \times 10^{-4}$		
19−23 (4)/GSH	1.08 ± 0.04	0.063 ± 0.008	3.0 ± 0.1	$\leq 2 \times 10^{-4}$
19−23 (4)/NEM	1.02 ± 0.04	0.056 ± 0.009	2.9 ± 0.2	$\leq 4 \times 10^{-4}$
19−23 (4)/NEM+GSH	1.04 ± 0.03	0.036 ± 0.003	3.1 ± 0.2	$\leq 6 \times 10^{-5}$
104−106 (2)/apo	2.01 ± 0.01	$\leq 2 \times 10^{-4}$		
104−106 (2)/GSH	1.07 ± 0.04	0.09 ± 0.01	1.00 ± 0.04	$\leq 2 \times 10^{-4}$
104−106 (2)/NEM	0.98 ± 0.02	0.029 ± 0.002	1.1 ± 0.1	$\leq 2 \times 10^{-4}$
104−106 (2)/NEM+GSH	0.95 ± 0.02	0.063 ± 0.003	1.08 ± 0.02	$\leq 2 \times 10^{-4}$
125−133 (7)/GSH	2.24 ± 0.07	0.060 ± 0.005	4.02 ± 0.01	$\leq 2 \times 10^{-4}$
125−133 (7)/GSH+PC	0.78 ± 0.01	0.21 ± 0.05	5.33 ± 0.05	$(1.23 \pm 0.05) \times 10^{-3}$
145−148 (3)/GSH	1.19 ± 0.08	0.24 ± 0.05	2.07 ± 0.06	$(2.3 \pm 0.2) \times 10^{-3}$
145−147 (3)/GSH+PC	1.16 ± 0.09	0.06 ± 0.01	2.06 ± 0.09	$\leq 4 \times 10^{-4}$

[a] Kinetic traces are illustrated in Figures 3 and 6A. [b] The numbers in parentheses are the total number of exchangeable sites. Unless otherwise noted, the exchange reactions were done in the presence of TX100 in the absence of GSH (apo), in the presence of GSH (GSH), after alkylation with NEM (NEM), and after alkylation with NEM in the presence of GSH (NEM+GSH). Exchange reactions done in the absence of TX100 and in the presence of GSH and phosphatidylcholine are denoted GSH+PC.

tional change and provides clear and direct evidence that the cytosolic domain of the enzyme harbors the GSH binding site.

Perhaps even more interesting is the behavior of two short peptides located roughly in the middle of helices 1 and 3 that show an increase in the exchange rate of a single amide in each peptide as shown in Figures 3B,C and 4A. The two sites exchange with similar kinetics (Table 1) suggesting that they are located in chemically similar environments. The precision of the kinetic data for peptides 19−23 and 104−106 suggests that the exchange at each of the two sites follows single-exponential kinetics with amplitudes of one deuterium per subunit. This is an important observation since this kinetic behavior is most consistent with a cooperative conformational transition in which all three subunits respond in a similar way to the binding of a single GSH/trimer. The alternative of only one of three subunits being influenced by the single GSH/trimer would be expected to lead to more complex exchange behavior such as double-exponential kinetics with amplitudes of less than one deuterium per subunit.

Each peptide, 19-ATIIL-23 and 104-IHF-106, harbors a hydrophilic side chain, which may facilitate solvent access to the helices after the conformational transition. Helical wheel projections of helices 1 and 3 (Figure 5) indicate that residues T20 and H105 reside on the faces of the two helices with the highest propensity for helical packing (*33*). We conclude that the H/D exchange kinetics constitutes the detection of an intersubunit or intrasubunit change in packing interactions involved in the cooperative conformational transition. The enhanced H/D exchange suggests that helical packing changes so that the hydrophilic faces have more access to solvent when GSH is bound. This cooperative transition may involve the reorientation of helices 1 and 3 in a manner that is reflected in the differences in helical inclinations observed in the *P*6 and $P22_12_1$ crystal forms (*9*). In the context of the three-dimensional density map, it seems most likely that the intersubunit contact is either between the A and C helices for an ABCD monomer grouping or the B and C helices for the ABC*D monomer grouping (Figure 1B).

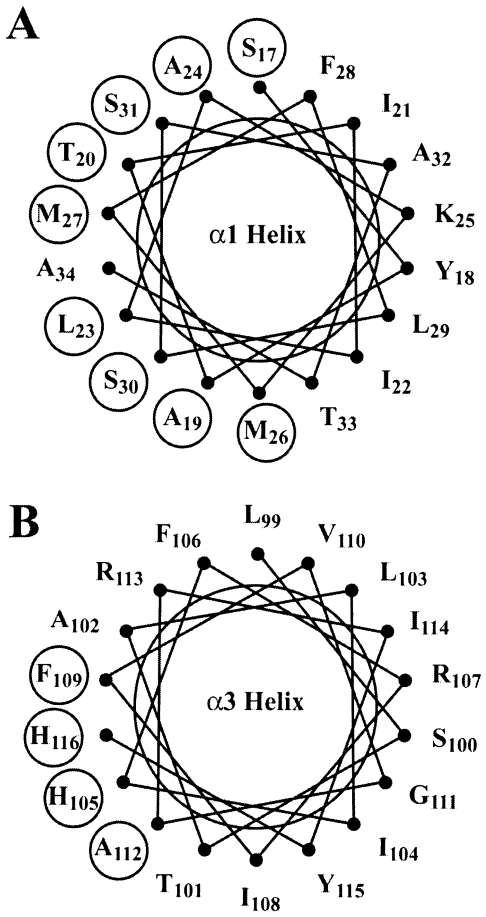

FIGURE 5: Helical wheel projections of helices 1 and 3 illustrating the faces predicted for transmembrane helix packing interactions. The transmembrane sequence was defined as the 18 most hydrophobic consecutive amino acid residues and the average helical packing values were calculated by the method of Liu and colleagues (33). Residues with average three-residue packing values greater than the predefined cutoff (0.45) were designated as having the greatest propensity for transmembrane packing interactions (circled). Note the location of T20 and H105 in these regions.

Conformational Response to Stress Sensor Modification. Alkylation of the chemical stress sensor (C49) with *N*-ethylmaleimide has a significant effect on the H/D exchange

kinetics and a small effect on the peptic digest where the peptide containing C49 is one residue shorter than the one derived from the native protein. In the absence of GSH, the NEM-alkylated protein aggregates, making it difficult to follow the exchange kinetics for extended periods of time. However data collected over a 2-h time course indicate that alkylation clearly alters the structure of the cytosolic domain as indicated in Figure 3A. Specifically, peptide 45−58, which contains C49, shows a decrease in the number of sites exchanging in both the fast and slow kinetic regimes. The addition of GSH to the NEM-alkylated enzyme produces an even more dramatic, additive decrease in the exchange rates of seven of the twelve sites. In contrast, peptide 75−90 at the junction of the cytosolic domain and helix-2 shows a substantial reduction in exchange in at least seven of the fourteen sites in the NEM-alkylated enzyme, which is substantially reversed upon addition of GSH.

Most striking is the fact that alkylation of C49 recapitulates the exchange behavior of peptides 19−23 in helix-1 and 104−106 in helix-3 observed for the native MGST1·GS$^-$ complex (Figures 3B,C and 4B). In addition, there is an increase in H/D exchange of one site in the middle of helix 4 (peptide 134−141, Figure S12A, Supporting Information) suggesting that alkylation in the absence of GSH changes the packing interactions in three of the four helices. Thus the alkylation event appears to loosen the packing interactions between the helices and therefore poises the protein near the cooperative transition associated with the binding and ionization of GSH at least with respect to the movements of the transmembrane helices. The influence of GSH on the exchange behavior of the NEM-modified protein is most pronounced in the cytosolic domain as illustrated in Figure 4C.

H/D Exchange in the Proteolipid Complex. Most of the detailed biochemical analysis of purified MGST1 has been done in the presence of the detergent Triton X-100, which forms a discrete complex with the protein. One salient issue with the H/D exchange analysis is to what extent the detergent complex reflects the behavior of the protein in the membrane. To address this issue, we carried out the H/D exchange experiments with proteolipid complexes containing catalytically active two-dimensional crystals of MGST1. The results are reported in Figure 6. Of the 147 main-chain N−H sites, only 13 exhibit altered kinetics in the proteolipid complex when compared to the TX100 complex. Nine of these sites are located in peptides near the predicted ends of the transmembrane helices where the zwitterionic phospholipid headgroups are expected to contact the protein. The other sites are located in the cytosolic domain and suggest that part of this domain may contact the membrane surface. However, the subtle differences indicate that the detergent and phospholipid complexes are structurally similar.

Conclusions. Our results are consistent with a catalytic mechanism for MGST1 involving a cooperative conformational transition that is coupled to the ionization of a single molecule of GSH per homotrimer. The binding of GSH leads to a more ordered structure, particularly in the cytosolic domain. The H/D exchange kinetics also suggest that reorientation of at least two of the transmembrane helices occurs during this transition and that the kinetic barrier for the event is lowered by chemical modification of the stress sensor, C49. The stress sensor appears to function as a molecular switch poising the protein in a conformation more favorable for binding and ionization of GSH. Finally, on a more general note, we have demonstrated that amide H/D exchange MS is a sensitive and attractive tool for examining the structure and dynamics of integral membrane proteins in both detergent and phospholipid complexes that are often difficult to study by other physical techniques.

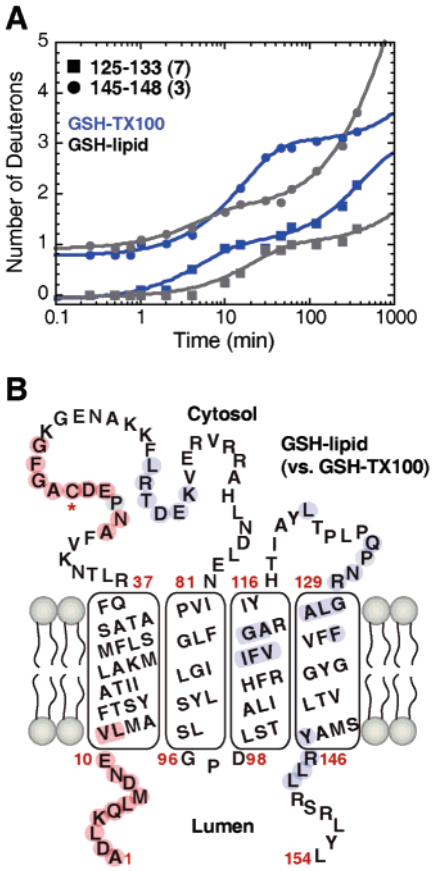

FIGURE 6: Kinetic profiles for peptide 125−133 (■) and segment 145−148 (●) from MGST1·GS$^-$·TX100 (blue) or from MGST1·GS$^-$·phosphatidylcholine (black). Numbers in parentheses are the total number of exchangeable sites. Summary of changes of the H/D exchange kinetics of MGST1·GS$^-$·phosphatidylcholine are referenced to MGST1·GS$^-$·TX100. Peptides colored in red and blue indicate enhanced and reduced exchange, respectively.

ACKNOWLEDGMENT

We thank Dr. David Hachey in the Mass Spectrometry Research Center Core Facilities for his advice and assistance with the mass spectrometry.

SUPPORTING INFORMATION AVAILABLE

Figures S1−S17 describing the peptic peptide map of the protein and rate constants and kinetic profiles for H/D exchange for all peptides. This material is available free of charge via the Internet at http://pubs.acs.org.

REFERENCES

1. Jakobsson, P.-J., Morgenstern, R., Mancini, J., Ford-Hutchinson, A., and Persson, B. (1999) Common structural features of MAPEG-A widespread superfamily of membrane associated proteins in eicosanoid and glutathione metabolism, *Protein Sci. 8*, 689−692.
2. Mosialou, E., Piemonte, F., Andersson, C., Vos, R. M. E., van Bladeren, P. J., and Morgenstern, R. (1995) Microsomal glu-

tathione transferase: Lipid-Derived Substrates and Lipid Dependence, *Arch. Biochem. Biophys. 320*, 210−216.
3. Kelner, M. J., Bagnell, R. D., Montoya, M. A., Estes, L. A., Forsberg, L., and Morgenstern, R. (2000) Structural organization of the microsomal glutathione *S*-transferase gene (*MGST1*) on chromosome 12p13.1−13.2. Identification of the correct promoter region and demonstration of transcriptional regulation in response to oxidative stress, *J. Biol. Chem. 275* 13000−13006.
4. Svensson, R., Rinaldi, R., Swedmark, S., and Morgenstern, R. (2000) Reactivity of cysteine-49 and its influence on the activation of microsomal glutathione transferase 1: Evidence for subunit interaction, *Biochemistry 39*, 15144−15149.
5. Sun, T.-H., and Morgenstern, R. (1997) Binding of glutathione and an inhibitor to microsomal glutathione transferase, *Biochem. J. 326*, 193−196.
6. Morgenstern, R., Svensson, R. Bernat, B. A., and Armstrong, R. N. (2001) Kinetic analysis of the slow ionization of glutathione by microsomal glutathione transferase MGST1, *Biochemistry 40*, 3378−3384.
7. Lengqvist, J., Svensson, R., Evergren, E., Morgenstern, R., and Griffiths, W. J. (2004) Observation of an Intact Noncovalent Homotrimer of Detergent-solubilized Rat Microsomal Glutathione Transferase-1 by Electrospray Mass Spectrometry, *J. Biol. Chem. 279*, 13311−13316.
8. Svensson, R., Ålander, J., Armstrong, R. N., and Morgenstern, R. (2004) Kinetic characterization of thiolate anion formation and chemical catalysis of activated microsomal glutathione transferase 1, *Biochemistry 43*, 8869−8877.
9. Schmidt-Krey, I., Mitsuoka, K., Hirai, T., Murata, K., Cheng, Y., Fujiyoshi, Y., Morgenstern, R., and Hebert, H. (2000) The three-dimensional map of microsomal glutathione transferase 1 at 6 Å resolution, *EMBO J. 19*, 6311−6316.
10. Holm, P. J., Morgenstern, R., and Hebert, H. (2002) The 3-D structure of microsomal glutathione transferase 1 at 6 Å resolution as determined by electron crystallography of p22121 crystals, *Biochim. Biophys. Acta 1594*, 276−285.
11. Englander, J. J., Rogero, J. R., and Englander, S. W. (1985) Protein hydrogen exchange studied by the fragment separation method, *Anal. Biochem. 147*, 234−244.
12. Zhang, Z., and Smith, D. L. (1993) Determination of amide hydrogen exchange by mass spectrometry: a new tool for protein structure elucidation, *Protein Sci. 2*, 522−531.
13. Johnson, R. S., and Walsh, K. A. (1994) Mass spectrometric measurement of protein amide hydrogen exchange rates of apo- and holo-myoglobin, *Protein Sci. 3*, 2411−2418.
14. Hoofnagle, A. N., Resing, K. A., and Ahn, N. G. (2003) Protein analysis by hydrogen exchange mass spectrometry, *Annu. Rev. Biophys. Biomol. Struct. 32*, 1−25.
15. Demmers, J. A. A., van Duijn, E., Haverkamp, J., Greathouse, D. V., Koeppe, R. E., 2nd, Heck, A. J., and Killian, J. A. (2001) Interfacial positioning and stability of transmembrane peptides in lipid bilayers studied by combining hydrogen/deuterium exchange and mass spectrometry, *J. Biol. Chem. 276*, 34501−34508.
16. Morgenstern, R., Guthenberg, C., and Depierre, J. W. (1982) Microsomal glutathione S-transferase. Purification, initial characterization and demonstration that it is not identical to the cytosolic glutathione S-transferases A, B and C, *Eur. J. Biochem. 128*, 243−248.
17. Riddles, P. W., Blakeley, R. L., and Zerner, B. (1983) Reassessment of Ellman's reagent, *Methods Enzymol. 91*, 49−60.
18. Schmidt-Krey, I., Lundqvist, G., Morgenstern, R., and Hebert, H. (1998) Parameters for the Two-Dimensional Crystallization of the Membrane Protein Microsomal Glutathione Transferase, *J. Struct. Biol. 123*, 87−96.
19. Hebert, H., Schmidt-Krey, I., and Morgenstern, R. (1995) The projection structure of microsomal glutathione transferase, *EMBO J. 14*, 3864−3869.
20. Schmidt-Krey, I., Murata, K., Hirai, T., Mitsuoka, K., Cheng, Y., Morgenstern, R., Fujiyoshi, Y., and Hebert, H. (1999) The projection structure of the membrane protein microsomal glutathione transferase at 3 Å resolution as determined from two-dimensional hexagonal crystals, *J. Mol. Biol. 288*, 243−253.
21. Henderson, R., Baldwin, J. M., Downing, K. H., Lepault, J., and Zemlin, F. (1986) Structure of purple membrane from halobacterium halobium: recording, measurement and evaluation of electron micrographs at 3.5 Å resolution, *Ultramicroscopy 19*, 147−178.
22. Fujiyoshi, Y., Mizusaki, T., Morikawa, K., Yamagishi, H., Aoki, Y., Kihara, H., and Harada, Y. (1991) Development of a superfluid helium stage for high-resolution electron microscopy, *Ultramicroscopy 38*, 241−251.
23. Wilkins, M. R., Lindskog, I., Gasteiger, E., Bairoch, A., Sanchez, J. C., Hochstrasser, D. F., and Appel, R. D. (1997) Detailed peptide characterization using PEPTIDEMASS- -a World-Wide-Web-accessible tool, *Electrophoresis 18*, 403−408.
24. Clauser K. R., Baker, P. R., and Burlingame, A. L. (1999) Role of accurate mass measurement (±10 ppm) in protein identification strategies employing MS or MS/MS and database searching, *Anal. Chem. 71*, 2871−2882.
25. Morgenstern, R., and DePierre, J. W. (1983) Microsomal glutathione transferase. Purification in unactivated form and further characterization of the activation process, substrate specificity and amino acid composition. *Eur. J. Biochem. 134*, 591−597.
26. Codreanu, S. G., Ladner, J. E., Xiao, G., Stourman, N. V., Hachey, D. L., Gilliland, G. L., and Armstrong, R. N. (2002) Local protein dynamics and catalysis: detection of segmental motion associated with rate-limiting product release by a glutathione transferase, *Biochemistry 41*, 15161−15172.
27. Zhang, Z., and Marshall, A. G. (1998) A universal algorithm for fast and automated charge state deconvolution of electrospray mass-to-charge ratio spectra, *J. Am. Soc. Mass. Spectrom. 9*, 225−233.
28. Henderson, R., Baldwin, J. M., Downing, K. H., Lepault, J., and Zemlin, F. (1986) Structure of purple membrane from halobacterium halobium: recording, measurement and evaluation of electron micrographs at 3.5 Å resolution, *Ultramicroscopy 19*, 147−178.
29. Collaborative Computational Project, Number 4 (1994) The CCP4 Suite: Programs for Protein Crystallography, *Acta Crystallogr. D50*, 760−763.
30. Jones, T. A., Zou, J. Y., Cowan, S. W., and Kjeldgaard, M. (1991) Improved methods for building protein models in electron density maps and the location of errors in these models, *Acta Crystallogr. A47*, 110−119.
31. Harris, M., and Jones, T. A. (2001) Molray − A web interface between O and the POV−Ray ray tracer, *Acta Crystallogr. D57*, 1201−1203.
32. Persistence of Vision Raytracer, http://www.povray.org.
33. Liu, W., Eilers, M., Patel, A. B., and Smith, S. O. (2004) Helix packing moments reveal diversity and conservation in membrane protein structure, *J. Mol. Biol. 337*, 713−729.

BI048716K